Available online at www.sciencedirect.com
SCIENCE DIRECT
Journal of Photochemistry and Photobiology A: Chemistry 176 (2005) 218–230
Journal of Photochemistry and Photobiology A:Chemistry
www.elsevier.com/locate/jphotochem

Theoretical studies of the reaction of hydroperoxy radicals ($HO_2^\bullet$) with ethyl peroxy ($CH_3CH_2O_2^\bullet$), acetyl peroxy ($CH_3C(O)O_2^\bullet$), and acetonyl peroxy ($CH_3C(O)CH_2O_2^\bullet$) radicals

Alam S. Hasson [a,*], Keith T. Kuwata [b], Manuel C. Arroyo [a], Erin B. Petersen [b]

[a] *Department of Chemistry, 2555 East San Ramon Avenue M/S SB70, California State University Fresno, CA 93740-8034, USA*
[b] *Department of Chemistry, Macalester College, 1600 Grand Avenue, St. Paul, MN 55105-1899, USA*

Received 8 July 2005; received in revised form 9 August 2005; accepted 9 August 2005
Available online 5 October 2005

Abstract

Product yield studies indicate that the reaction of organic peroxy radicals ($RO_2^\bullet$) with hydroperoxy radicals ($HO_2^\bullet$) may proceed via four reaction channels:

$$RO_2^\bullet + HO_2^\bullet \rightarrow ROOH + O_2 \quad \text{(R1a)}$$

$$RO_2^\bullet + HO_2^\bullet \rightarrow ROH + O_3 \quad \text{(R1b)}$$

$$RO_2^\bullet + HO_2^\bullet \rightarrow RO^\bullet + {}^\bullet OH + O_2 \quad \text{(R1c)}$$

$$RO_2^\bullet + HO_2^\bullet \rightarrow R'CHO + H_2O + O_2 \quad \text{(R1d)}$$

While (R1a) is the dominant pathway for alkyl peroxy radicals, it has been reported that acetyl peroxy radicals ($R = CH_3C(O)$) react via (R1a), (R1b) and (R1c), while acetonyl peroxy radicals ($R = CH_3C(O)CH_2$) reacts via (R1a) and (R1c). In this work, quantum calculations using the CBS-QB3 method coupled with Master equation analysis and kinetic simulations have been used to propose reaction mechanisms for the formation of the products observed in reaction (R1) for ethyl peroxy ($R = CH_3CH_2$), acetyl peroxy, and acetonyl peroxy radicals. (R1a) is found to proceed via hydrogen atom transfer, while (R1b) and (R1c) both proceed through a hydrotetroxide intermediate. The calculations demonstrate that the mechanism is consistent with the experimentally measured product yields, and that (R1b) and (R1c) may also be significant for structurally similar organic peroxy radicals. The implications of these calculations are discussed.

Keywords: Air pollution; Peroxy radicals; Reaction mechanisms; Electronic structure calculations; Reaction kinetics

1. Introduction

Organic peroxy radicals ($RO_2^\bullet$) are key intermediates in the atmospheric degradation of organic compounds [1,2]. The reaction of primary organic pollutants with tropospheric oxidants such as hydroxy radicals ($^\bullet OH$) and ozone (O_3) invariably leads to the formation of an alkyl radical, which then reacts with oxygen to form $RO_2^\bullet$. Acetyl peroxy radicals ($R = CH_3C(O)–$) are generated in the initial stages of the oxidation of a number of important atmospheric pollutants including acetaldehyde, acetone, and some internal alkenes. They may also be formed in the troposphere from the oxidation products of many primary organic pollutants, such as isoprene and propene. Acetonyl peroxy radicals ($R = CH_3C(O)CH_2–$) are intermediates formed in the oxidation of acetone.

* Corresponding author. Tel.: +1 559 278 2420; fax: +1 559 278 4402.
E-mail address: ahasson@csufresno.edu (A.S. Hasson).

1010-6030/$ – see front matter © 2005 Elsevier B.V. All rights reserved.
doi:10.1016/j.jphotochem.2005.08.012

Table 1
Summary of branching ratios measured for $RO_2^\bullet + HO_2^\bullet$ reactions

$RO_2^\bullet$ radical	Y_{R1a}	Y_{R1b}	Y_{R1c}	Y_{R1d}	Reference
C_1–C_6 alkyl peroxy	≥0.89	≤0.11	–	–	[3–11]
$CH_2FO_2^\bullet$	0.29	–	–	0.71	[15]
$CH_3OCH_2O_2^\bullet$	0.60	–	–	0.40	[14]
$CH_2ClO_2^\bullet$	0.27	–	–	0.73	[17]
$CHCl_2O_2^\bullet$	–	–	–	1[b]	[16]
$CCl_3O_2^\bullet$	–	–	–	1[b]	[16]
$CH_3C(O)O_2^\bullet$	≈0.75[a]	≈0.25[a]	–	–	[18–22]
	0.4	0.2	0.4	–	[10]
$CF_3CF_2C(O)O_2^\bullet$	–	0.24	0.76	–	[23]
$CH_3C(O)CH_2O_2^\bullet$	1	–	–	–	[54]
	0.33	–	0.67	–	[10]

[a] Relative branching ratios of (R1a) and (R1b); (R1c) was not considered.
[b] Reaction proceeds via (R1d′): $CXCl_2O_2^\bullet + HO_2^\bullet \rightarrow XC(O)Cl + HOCl + O_2$.

Reactions between $RO_2^\bullet$ and hydroperoxy radicals ($HO_2^\bullet$) represent an important sink for $RO_2^\bullet$ (R1a)–(R1d), particularly under low NO_x conditions ($NO_x = NO + NO_2$).

$$RO_2^\bullet + HO_2^\bullet \rightarrow ROOH + O_2 \quad \text{(R1a)}$$

$$RO_2^\bullet + HO_2^\bullet \rightarrow ROH + O_3 \quad \text{(R1b)}$$

$$RO_2^\bullet + HO_2^\bullet \rightarrow RO^\bullet + {}^\bullet OH + O_2 \quad \text{(R1c)}$$

$$RO_2^\bullet + HO_2^\bullet \rightarrow R'CHO + H_2O + O_2 \quad \text{(R1d)}$$

Experimentally, four sets of products have been identified from reaction (R1), as summarized in Table 1. A number of unsubstituted alkyl peroxy radicals have been shown to form organic hydroperoxides (ROOH, (R1a)) with a yield of almost unity [3–11]. ROOH typically have lifetimes in excess of 24 h, and may be removed from the atmosphere before they undergo additional chemical processes [12,13]. Reaction (R1a) thus serves as a chemical sink for peroxy radicals.

More complex $RO_2^\bullet$ may undergo additional reactions (R1b)–(R1d). These reactions are potentially important because they lead to products that may undergo further chemical reactions before they are removed from the atmosphere. Thus, air pollution models that do not include this additional chemistry may underestimate levels of secondary pollutants such as ozone. Wallington and co-workers have shown that radical species of the form $CH_nX_{(3-n)}OO^\bullet$ (where $n = 1$–3 and X = F, Cl, and CH_3O) react to form carbonyl compounds via (R1d) with yields ranging from 0.4 to 1 [14–17]. Additionally, a number of researchers have reported that organic peroxy radicals of the form $RC(O)O_2^\bullet$ (R = CH_3 and CF_3) react via (R1b) to form a carboxylic acid and ozone with yields of around 0.25 [18–22].

More recently, evidence has been found that $CH_3C(O)O_2^\bullet$, $CH_3C(O)CH_2O_2^\bullet$, and $CF_3C(O)O_2^\bullet$ may react to form an alkoxy radical ($RO^\bullet$) and $^\bullet OH$ (R1c) with yields as high as 0.76 [10,23]. In contrast to the majority of organic peroxy radicals, reaction (R1c) is exothermic for both $CH_3C(O)O_2^\bullet$ [24] and $CF_3C(O)O_2^\bullet$ [23]. However, this reaction is endothermic for $CH_3C(O)CH_2O_2^\bullet$ [24], and so it is surprising that (R1c) is found to be the dominant reaction for this radical.

Until recently, the mechanisms of $RO_2^\bullet + HO_2^\bullet$ reactions were unknown. It had been speculated, however, that the reaction is analogous to the $RO_2^\bullet + RO_2^\bullet$ reaction, and proceeds via a hydrotetroxide intermediate, e.g. [19]. Indirect experimental evidence for the formation of this intermediate is provided by the negative temperature dependence of the rate coefficient for (R1) observed for a number of $RO_2^\bullet$ species ([24] and references therein). If formed, the hydrotetroxide intermediate could generate all of the observed products from these reactions [19], as illustrated in the scheme below for the products observed for the acetyl peroxy reaction.

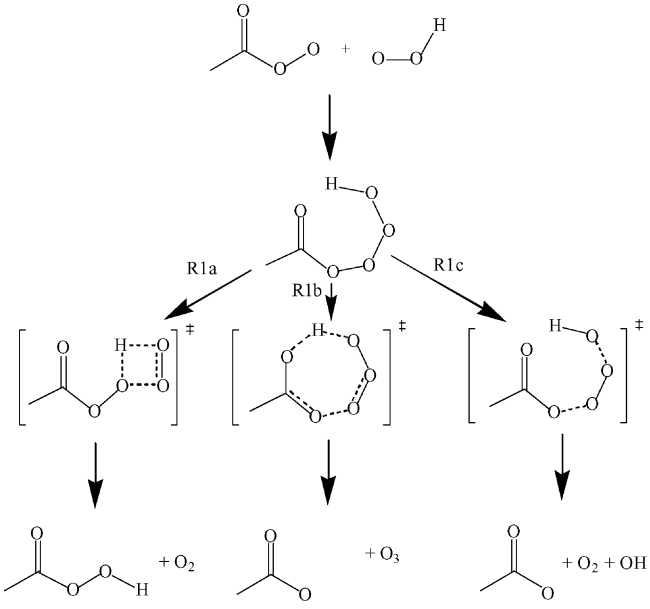

Recently, Hou and Wang carried out the first computational study on $RO_2^\bullet + HO_2^\bullet$ reactions [25]. The authors report data for the reactions of methyl peroxy ($CH_3O_2^\bullet$) and fluoromethyl peroxy ($CH_2FO_2^\bullet$) radicals. In both cases, formation of the hydroperoxide (R1a) is found to proceed via the formation of a hydrogen-bonded complex rather than the hydrotetroxide. This complex then undergoes a hydrogen atom transfer to form the observed products. The formation of CHFO from $CH_2FO_2^\bullet$ does, however, involve the hydrotetroxide intermediate.

In this study, the mechanism of reaction (R1) for ethyl peroxy, acetyl peroxy, and acetonyl peroxy radicals has been investigated. Quantum calculations were performed to identify the geometries, vibrational frequencies, and energies of reactants, transition states, intermediates, and products. Master equation calculations and kinetic simulations were also carried out to demonstrate that the proposed pathways are consistent with experimentally measured product yields from reaction (R1). The implications of these results for other $RO_2^\bullet + HO_2^\bullet$ reactions are discussed.

2. Calculation methods

2.1. Quantum chemistry calculations

All electronic structure calculations were performed with the Gaussian 03 program suite [26]. Optimized geometries for all minima and transition states were obtained at the B3LYP/6-311G(2d,d,p) level of theory. The harmonic vibrational frequencies for these structures were then determined at the same level of theory; all of the vibrational frequencies for reported minima are real, while reported transition states contain one imaginary frequency. Transition states were associated with specific reactants and products both by animation of the imaginary frequency and intrinsic reaction coordinate (IRC) calculations [27,28].

The energies of all structures were determined using the CBS-QB3 method, with relative energies being corrected for differences in zero-point vibrational energy scaled by 0.99 [29]. Studies indicate that CBS-QB3 often provides excellent agreement with experimental barrier heights and thermodynamic parameters [30–34]. A recent benchmarking study by Dybala-Defratyka et al. [35] suggests that errors in CBS-QB3 atomization energies are ∼2 kcal/mol. Radom and co-workers [36,37] have provided evidence that the standard CBS-QB3 method may overcompensate for the effect of spin contamination on the energies of doublet systems. We are not aware of any similar evaluations of the CBS-QB3 spin correction term for triplet or open shell singlet systems, the predominant types of electronic structure in the current study. Given that spin contamination undoubtedly introduces systematic error in our calculations, we decided to accept the standard CBS-QB3 correction for this error. The rigorous way to avoid spin contamination completely would be to perform multireference calculations on our species [38], but the cost of treating both static and dynamic electron correlation properly is still prohibitive for systems of our size. To aid in our analysis, we also determined partial charges for some structures by natural population analysis (NPA) at the B3LYP/6-311G(2d,d,p) optimized geometries. NPA charges were computed using the NBO 3.1 program [39].

2.2. Kinetic calculations

Master equation calculations were performed using the MULTIWELL suite of programs [40,41], as used in previous work [33,34,42]. Within the MULTIWELL program, B3LYP/6-311G(2d,d,p) vibrational frequencies and rotational constants, and CBS-QB3 barrier heights were used to calculate unimolecular rate coefficients using RRKM theory. Several of the reactions were found to proceed through loose transition states that do not have well-defined geometries. MULTIWELL cannot calculate rate coefficients for these reactions, and so these data were incorporated into the Master equation calculations using an external file of rate coefficients. These were calculated by microcanonical transition state theory using the minimum sum of states criterion [43]. For each reaction, the minimum sum of states was determined as the distance along the reaction coordinate was varied. Vibrational frequencies in the reactant molecule that are correlated with vibrations in the separated fragments were assumed to have the functional form:

$$v(r) = v(r_e)\exp(-\alpha(r - r_e)) + v_\infty(1 - \exp(-\alpha(r - r_e))) \quad \text{(E1)}$$

where r is the distance between the separating fragments, r_e is the distance between the fragments in the parent molecule, $v(r)$ is the vibrational frequency at distance r, $v(r_e)$ is the vibrational frequency in the parent molecule, v_∞ is the vibrational frequency in the separated fragments and α is an adjustable parameter, which was set to $1\,\text{Å}^{-1}$ [43]. Transitional frequencies in the parent molecule were assumed to have the same functional form, but with v_∞ set equal to zero. A Morse potential with a Morse parameter of 1.9 Å was assumed for the electronic potential energy [43]. In previous work, calculated product yields were found to be fairly insensitive to both the Morse parameter and α [34].

The exponential-down model was used in the simulations for collisional energy transfer. The average energy transferred per collision was assumed to be $300\,\text{cm}^{-1}$. Lennard–Jones parameters for the reactants are unknown, and were therefore estimated from literature values for similar molecules [33,44].

Tunneling was not considered in our calculations. Treatment of tunneling would increase the predicted rate of hydrogen transfer reactions, particularly those with tighter transition states. This is the situation with **TS17-A**. Our lowering of the energy of **TS17-A** to reproduce experimental branching ratios in the simulations described below is roughly equivalent to a treatment of tunneling.

MULTIWELL uses a stochastic method to solve the Master equation. In this work, 1000 stochastic trials were performed to determine each reported result. The number of simulations was varied for several of the calculations to ensure that the number of trials did not systematically affect the values obtained. Each stochastic trial was run until the molecule had undergone 1000 collisions. This number was varied in several calculations to ensure the reaction system had reached pseudo steady state by the end of the simulations.

For all of the reactions studied, the mechanism is found to branch at the initial bimolecular reaction step between the $RO_2^\bullet$ and $HO_2^\bullet$ radicals. The relative rates of these bimolecular reactions were determined from the thermal rate coefficient for the reverse unimolecular process and the equilibrium constant for the reaction, determined from the thermodynamic parameters of the reactants and products from the CBS-QB3 calculations.

Some additional kinetics simulations were carried out for collisionally stabilized species using the FACSIMILE computer program [45]. Thermal rate coefficients obtained from the MULTIWELL calculations were incorporated into the kinetic rate equations for the reaction mechanism. These sets

of differential equations were then numerically integrated using FACSIMILE.

3. Results and discussion

3.1. Quantum chemistry calculations

3.1.1. $C_2H_5O_2^\bullet + HO_2^\bullet$

The reaction mechanism determined from the CBS-QB3 calculations is shown in Fig. 1. Optimized geometries for key species involved in this reaction are shown in Fig. 2. The calculations show that the reaction may proceed in two ways. First the ethyl peroxy radical (**1**) may hydrogen bond to the H-atom of the hydroperoxy radical (**2**) to form **6** (Path I). This species may then undergo hydrogen atom transfer via **TS7** to form the hydrogen-bonded complex **8**, which can dissociate to produce ethyl hydroperoxide (**9**) and molecular oxygen (**10**). Second, the hydrogen-bonded complex **3** may be formed, leading to the formation of the hydrotetroxide **5** via **TS4** (Path II). Paths III and III′ and (via **TS11** and **TS17**, respectively) potentially lead from **5** to ethoxy radicals (**13**), $^\bullet$OH (**16**), and O_2 (**10**) but the overall reaction is endothermic and is therefore unlikely to be a significant reaction pathway.

The NPA charges on the oxygen atoms of ethyl peroxy radical **1** (Fig. 2) indicate that, based solely on electrostatics, $HO_2^\bullet$ (**2**) may be expected to form a hydrogen bond with either oxygen atom. In both complex **3** and complex **6**, the hydrogen bond polarizes the electron density, increasing the negative charge on whichever oxygen is serving as the hydrogen bond acceptor. The H-bond acceptor atom in **3** is slightly more negatively charged than the H-bond acceptor atom in **6** because the ethyl group directly bonded to the O atom in **3** can donate some electron density to it by hyperconjugation. The slightly stronger electrostatic interaction in **3** versus **6** is consistent with **3**'s slightly greater stability.

Formation of ethyl hydroperoxide from the hydrotetroxide **5** through the four-membered cyclic transition state equiva-

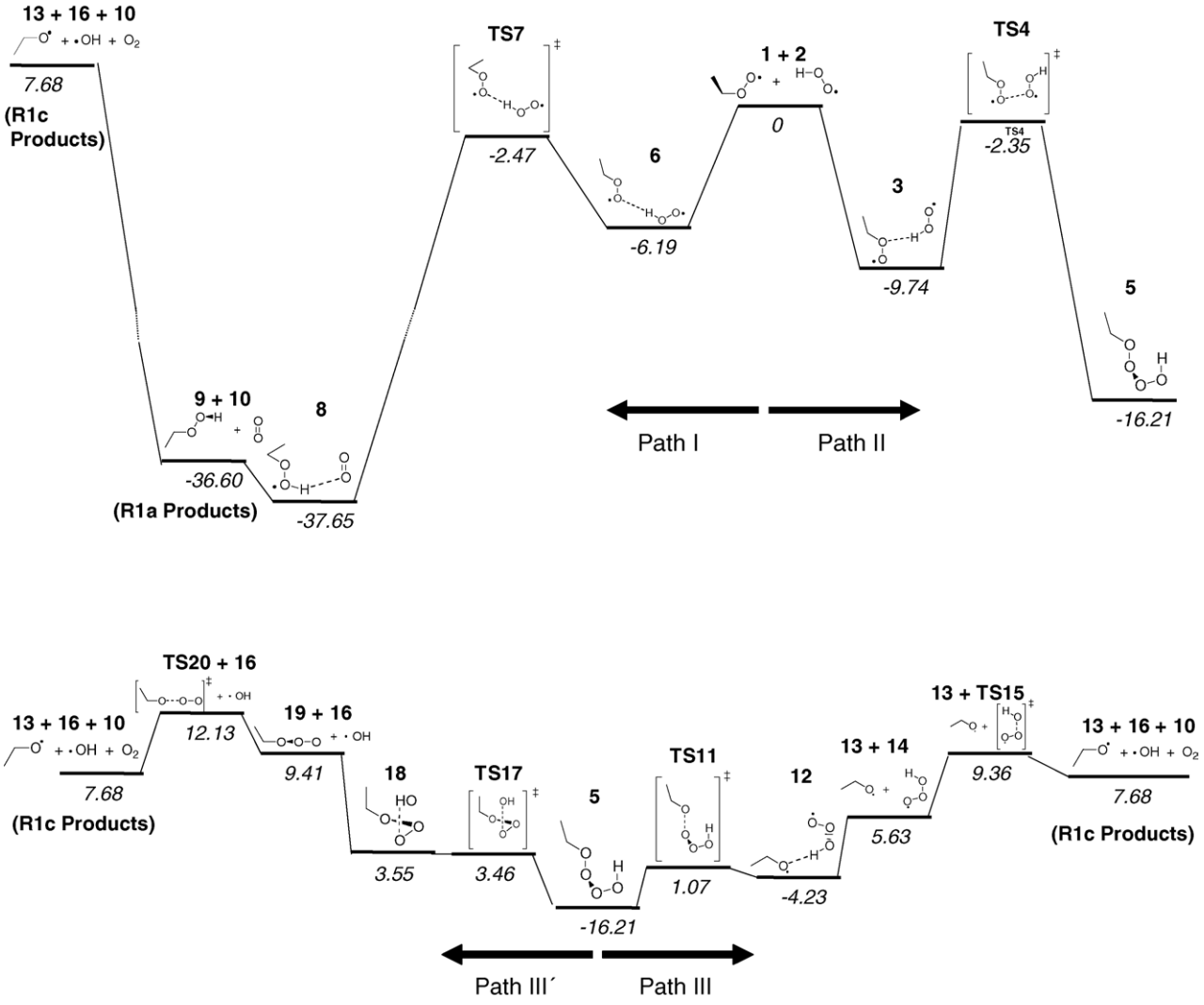

Fig. 1. Mechanism for the reaction of ethyl peroxy radicals (**1**) with hydroperoxy radicals (**2**) calculated by the CBS-QB3 method. Numbers below the structures are energies in kcal/mol relative to the energy of **1** + **2**. The *y*-axis is not drawn to scale.

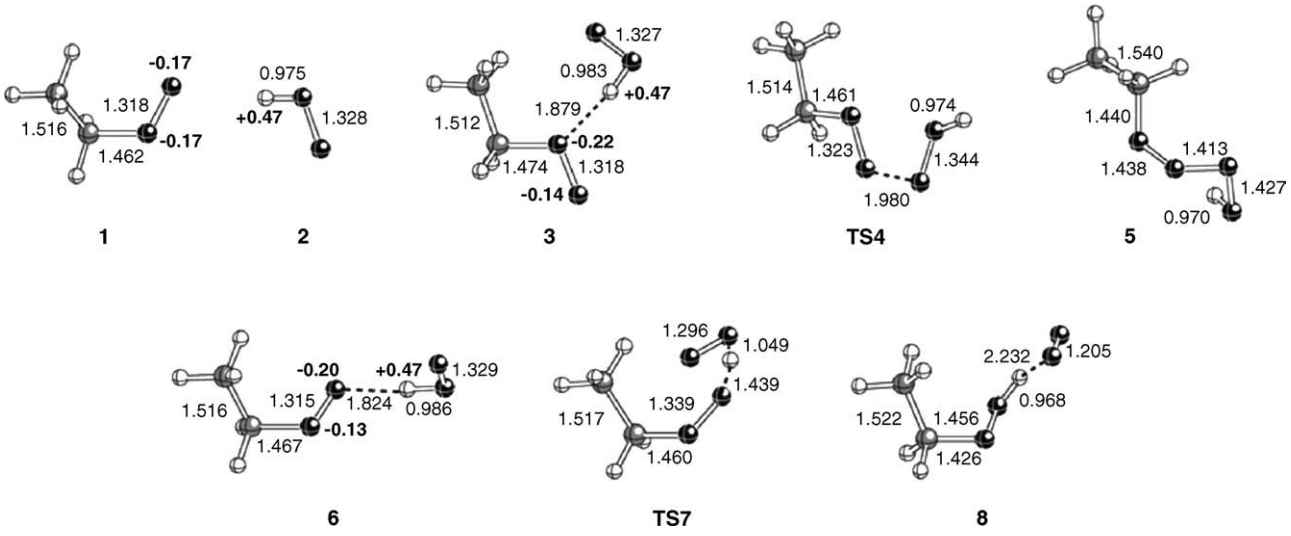

Fig. 2. Structures of key species in the reaction of ethyl peroxy radicals with hydroperoxy radicals determined by B3LYP/6-311G(2d,d,p) calculations. In all figures, bond lengths (in angstroms) are in normal type, selected natural population analysis charges are in bold type, grey represents carbon atoms, white represents hydrogen atoms, and black represents oxygen atoms.

lent to that shown in the reaction scheme in the Introduction is found to be even more energetically unfavorable than Paths III and III′. Extensive calculations did not reveal the existence of a transition state for (R1a) (the four-membered ring pathway to the hydroperoxide + O_2) on the B3LYP surface. The transition state is likely destabilized by the high degree of ring strain as well as repulsion between lone pairs. Since the reaction cannot proceed by this pathway, it is not shown in Fig. 1. The calculations reported here are consistent with data obtained by Hou and Wang [25] for the $HO_2^\bullet + CH_3O_2^\bullet$ reaction using the CCSD(T)/cc-pVDZ method. The authors report that the formation of a hydrogen-bonded complex analogous to **6** is exothermic by −7.65 kcal/mol. This species may then generate methyl hydroperoxide via a transition state with a barrier lower in energy than that of the reactants. Alternatively, the formation of the hydrotetroxide (analogous to **5**) is more exothermic (−9.22 kcal/mol), but the decomposition of this species occurs via pathways with substantial activation energies, and so these reactions are unlikely to occur. This conclusion is consistent with the high hydroperoxide yields measured experimentally [3,5–7,9].

3.1.2. $CH_3C(O)O_2^\bullet + HO_2^\bullet$

Fig. 3 shows the reaction mechanism determined from the electronic structure calculations, and Fig. 4 shows calculated geometries for the important species involved in the reaction. The initial stages of the reaction are equivalent to those of the ethyl peroxy reaction. Thus the acetyl peroxy radical (**1-A**) may undergo hydrogen atom transfer from $HO_2^\bullet$ (**2**) via the H-bonded complex **6-A** and **TS7-A** to form peracetic acid (**9-A**) and O_2 (**10**) (Path I-A). Alternatively, the reaction may lead to the formation of the hydrotetroxide **5-A** via **3-A** and **TS4-A** (Path II-A). Once formed, **5-A** may react via two different pathways. First, **5-A** may undergo homolytic O–O bond cleavage via **TS11-A** to form a hydrogen bonded complex (**12-A**) that can dissociate to form acetoxy radicals (**13-A**) and $HO_3^\bullet$ radicals (**14**) (Path III-A). The latter species may then dissociate to form $^\bullet$OH radicals (**16**) and O_2 (**10**). Second, **5-A** may isomerize via a seven-membered transition state (**TS17-A**) to form **18-A**, which can then dissociate to form acetic acid (**19-A**) and ozone (**20**) (Path IV-A). Transition state **TS17-A**, which involves the concerted breaking of an O–O bond and the formation of an O–H bond, may thus be classified as a 3,4-sigmatropic rearrangement. This novel pericyclic reaction has some precedence in the organic and organometallic literature [46–48].

The key difference between the mechanisms for ethyl peroxy and acetyl peroxy radicals is that Paths III and III′ are endothermic with respect to the reactants, whereas Paths III-A and IV-A are exothermic. Based on the quantum calculations, therefore, Paths I-A to IV-A all appear feasible, and can potentially explain the experimental product yields measured for the $CH_3C(O)O_2^\bullet + HO_2^\bullet$ reaction. Thus peracetic acid and oxygen (R1a) may be formed via Path I-A, acetic acid and ozone (R1b) may be formed via Path II-A followed by Path IV-A, while acetoxy radicals, $^\bullet$OH, and O_2 (R1c) may be generated via Path II-A followed by Path III-A. Interestingly, Moortgat et al. [19] speculated that acetic acid formation occurs by a mechanism equivalent to Paths II-A and IV-A in the late 1980s. Although this mechanism has become widely accepted, this study is, as far as we are aware, the first theoretical evidence for this mechanism using a rigorous computational approach.

An obvious structural difference between **5-A** and **5** is that the former molecule is capable of internal hydrogen bonding between the oxygen atom of the carbonyl group and the hydrogen atom of the hydrotetroxide group. This internal hydrogen bonding is also apparent in **TS11-A**, **12-A**, and

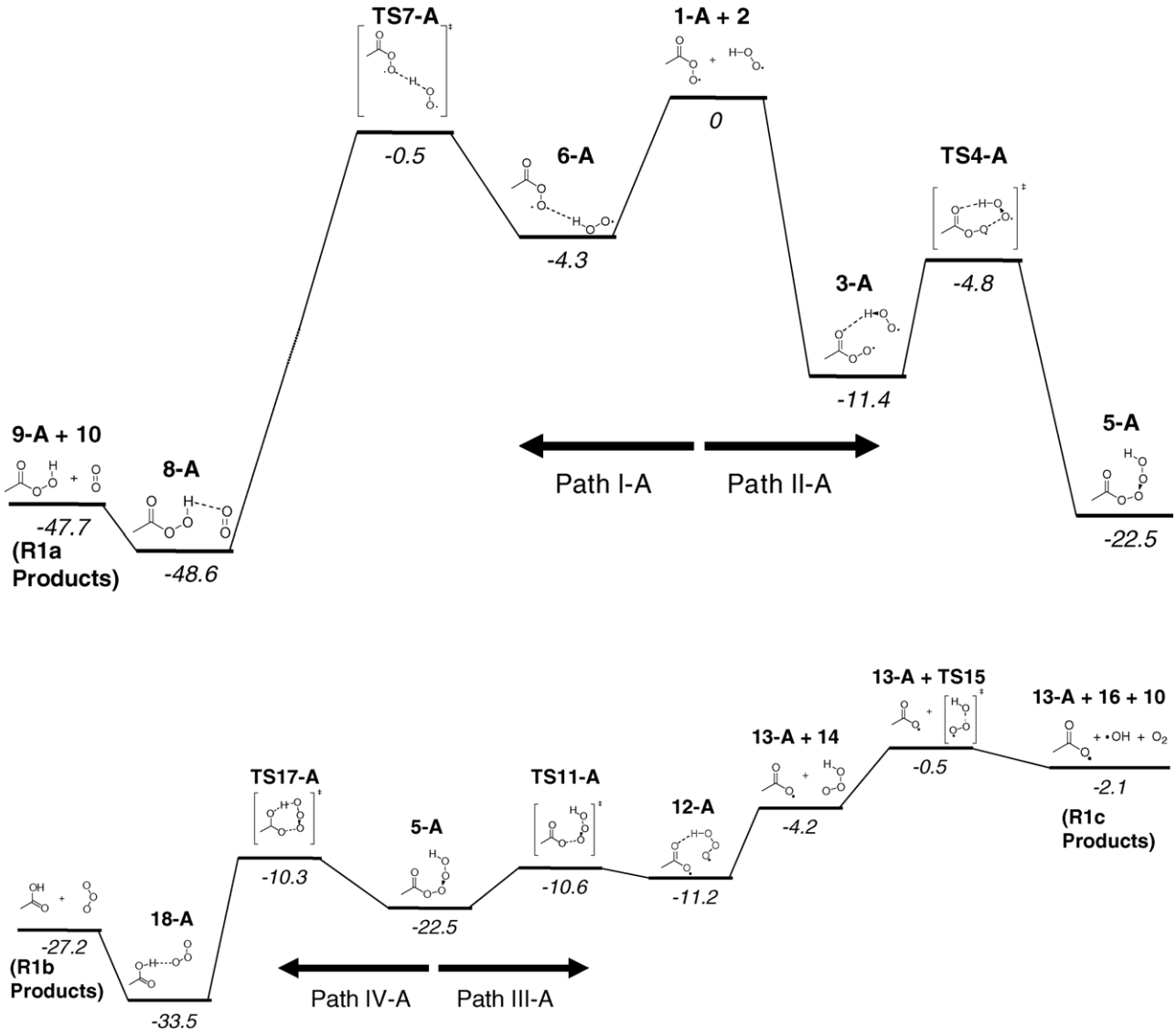

Fig. 3. Mechanism for the reaction of acetyl peroxy radicals (**1-A**) with hydroperoxy radicals (**2**) calculated by the CBS-QB3 method. Numbers below the structures are energies in kcal/mol relative to the energy of **1-A** + **2**. The *y*-axis is not drawn to scale.

TS17-A, as shown in Fig. 4. The effect appears critical in stabilizing these species, and therefore in reducing the activation energies for Paths III-A and IV-A. Evidence supporting the stabilization of reaction pathways via hydrogen bonding has been reported in the literature [49–52]. Natural population analysis indicates that the carbonyl oxygen in **1-A** (Fig. 4) is significantly more negatively charged than either of the oxygens in the peroxy group. Just as in the ethyl peroxy system, hydrogen bonding by $HO_2^\bullet$ to the acetyl peroxy radical polarizes the charge distribution compared to **1-A**; the carbonyl O in **3-A** is more negative by 0.05*e*, and the terminal peroxy O in **6-A** is more negative by 0.03*e*. The greater electron density on the hydrogen bond acceptor atom in **3-A** versus that in **6-A** helps explain why **3-A** is ∼7 kcal/mol more stable (according to CBS-QB3) than **6-A** (Fig. 3).

The acetoxy radical (**13-A**) produced via Path IVA is resonance stabilized, making the overall reaction thermodynamically favorable. It seems likely that the equivalent intermediates formed from the reaction of $HO_2^\bullet$ with larger acyl peroxy radicals (such as $C_2H_5C(O)O_2^\bullet$) will be stabilized in the same way, and they may also have significant yields of products from reaction (R1c). Likewise, the carbonyl oxygen of the larger acyl peroxy radicals should have similar basicities, making significant production of larger carboxylic acids and ozone (R1b) also possible. Further, it is possible that other peroxy radicals with an electronegative group (X) connected to the α-carbon atom ($RCHXO_2^\bullet$), may generate intermediates stabilized by internal hydrogen bonding, and therefore may also undergo reaction (R1c). These possibilities were not explored further in this work.

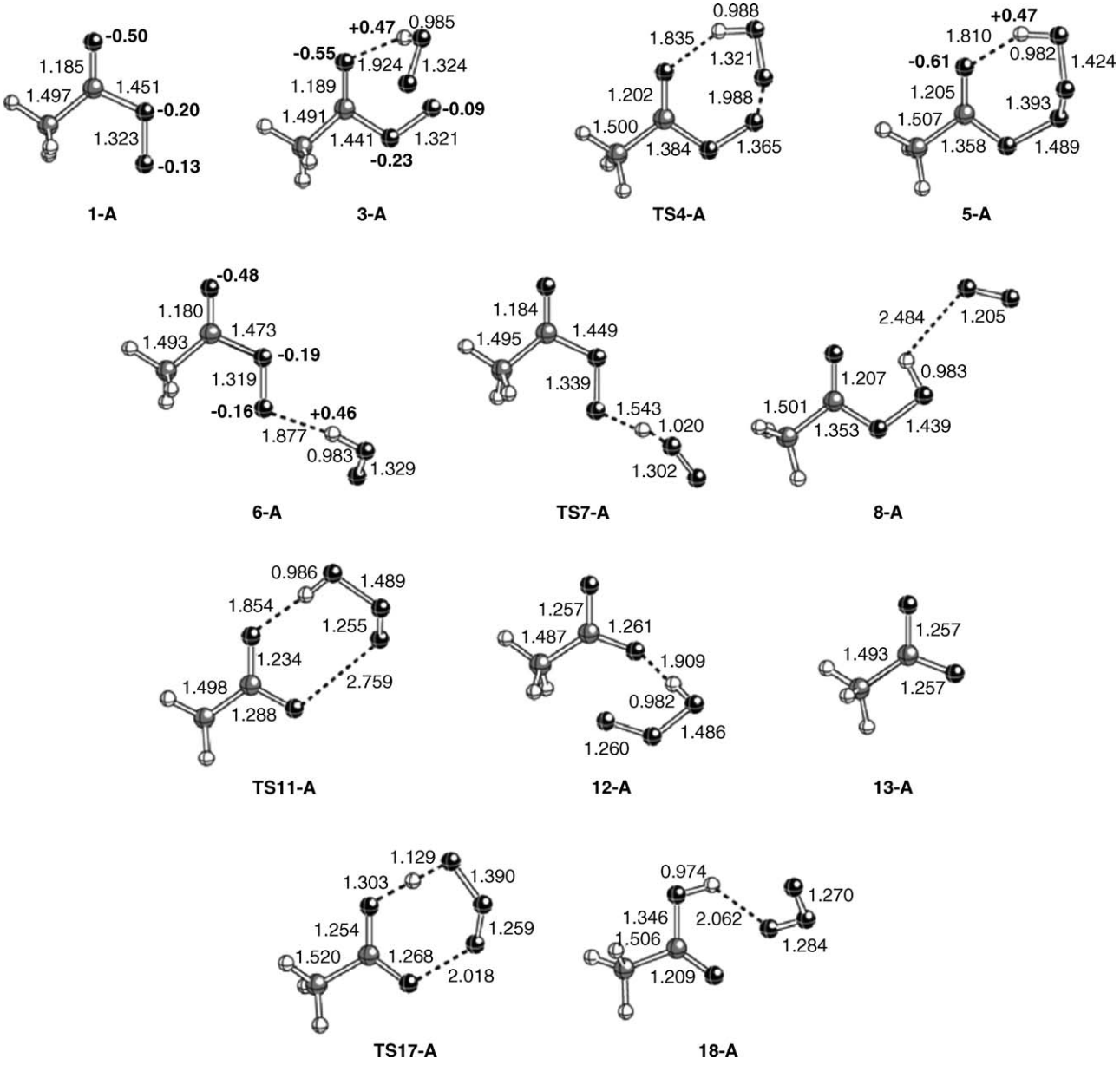

Fig. 4. Structures of key species in the reaction of acetyl peroxy radicals with hydroperoxy radicals determined by B3LYP/6-311G(2d,d,p) calculations.

3.1.3. $CH_3C(O)CH_2O_2^\bullet + HO_2^\bullet$

Results from the CBS-QB3 calculations for the acetonyl peroxy + $HO_2^\bullet$ reaction are shown in Figs. 5 and 6. The initial steps are analogous to those of the ethyl peroxy and acetyl peroxy reactions, resulting in the formation of acetonyl hydroperoxide (**9-B**) via Path I-B or the hydrotetroxide intermediate (**5-B**) via Path II-B. As with **5-A**, the intermediate **5-B** is stabilized by internal hydrogen bonding. Because the carbonyl group in **5-B** is not directly connected to the hydrotetroxide group, the concerted 3,4-sigmatropic rearrangement possible in **5-A** is precluded here. Therefore, **5-B** cannot decompose to form O_3 as **5-A** can.

The magnitudes of the NPA charges on the carbonyl oxygen and the terminal peroxy oxygen in **1-B** (Fig. 6) are larger than those on the analogous oxygen atoms in **1-A** (Fig. 4). As with the other systems, hydrogen bonding of $HO_2^\bullet$ to acetonyl peroxy increases the negative charge on both H-bond donor atoms. In complex **3-B**, the carbonyl oxygen has $-0.59e$, and in complex **6-B**, the terminal peroxy oxygen has $-0.20e$. These partial charges are larger in magnitude than in complexes **3-A** and **6-A** (Fig. 4), which helps explain why **3-B** and **6-B** are more strongly bound than their acetyl peroxy analogs.

The analogous $^\bullet$OH radical-forming pathway (homolytic O–O bond cleavage, which ultimately leads to the formation of the acetonoxy radical (**13-B**), $^\bullet$OH, and O_2) via Path III-B is endothermic for the acetonyl peroxy radical reaction. However, an alternative pathway leading to the formation of

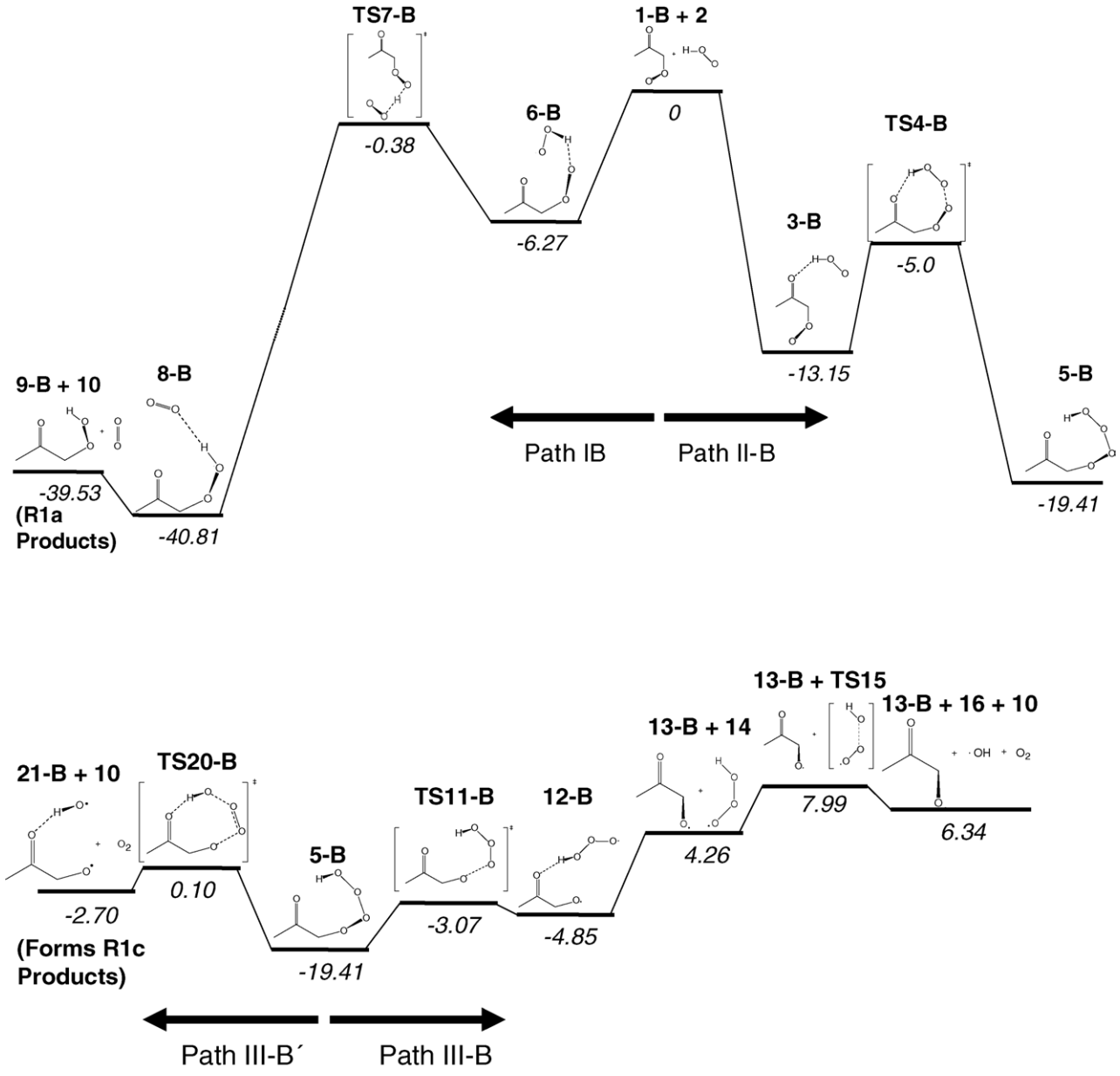

Fig. 5. Mechanism for the reaction of acetonyl peroxy radicals (**1-B**) with hydroperoxy radicals (**2**) calculated by the CBS-QB3 method. Numbers below the structures are energies in kcal/mol relative to the energy of **1-B** + **2**. The *y*-axis is not drawn to scale.

the same products but with lower barrier heights, Path III-B′, may also occur. In this reaction, O_2 is eliminated from the hydrotetroxide to produce a hydrogen-bonded complex between a hydroxy radical and an acetonoxy radical (**21-B**). While cleavage of the hydrogen bond to form $^{\bullet}$OH and acetonoxy radicals is endothermic, this unimolecular reaction may still be considerably faster than the reverse reaction between **21-B** and O_2. Thus the formation of $^{\bullet}$OH radicals (R1c) via Path II-B followed by Path III-B′ may be competitive with the formation of acetonyl hydroperoxide (R1a) via Path I-B. These pathways therefore provide a possible mechanism for formation of both the hydroperoxide (R1a) and $^{\bullet}$OH (R1c) from the reaction of acetonyl peroxy radicals with $HO_2^{\bullet}$, as reported in a recent experimental study [10] (see Table 1).

3.2. Kinetic calculations

The quantum calculations described above reveal plausible mechanisms via which the experimentally observed product yields may be formed in these three $RO_2^{\bullet} + HO_2^{\bullet}$ reactions. However, these calculations do not directly show whether or not the different reaction paths are competitive. To gain further insight into these reactions, Master equation calculations and kinetics simulations were performed. Because of uncertainties associated with several of the parameters in

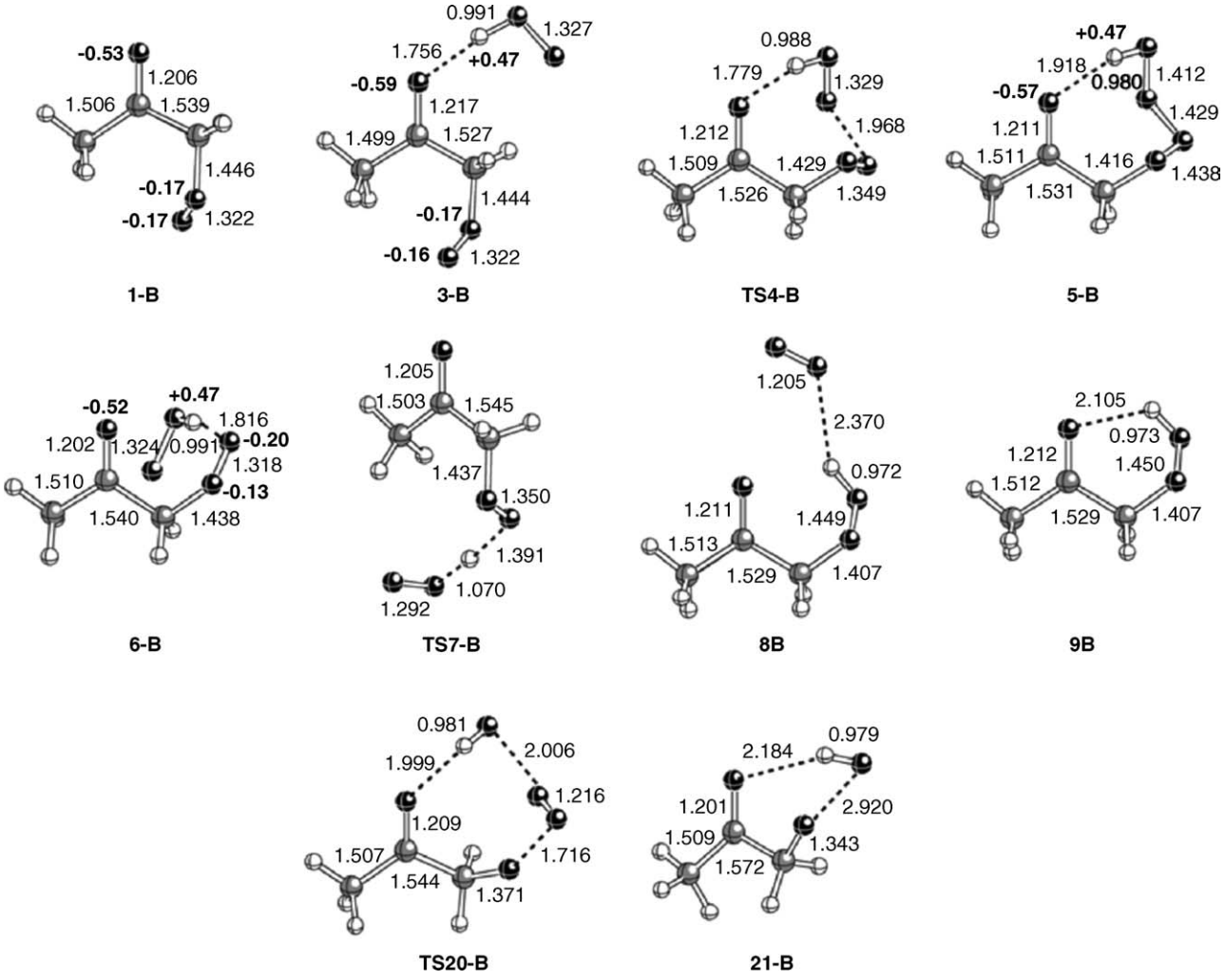

Fig. 6. Structures of key species in the reaction of acetonyl peroxy radicals with hydroperoxy radicals determined by B3LYP/6-311G(2d,d,p) calculations.

these calculations, exact quantitative agreement with experimentally observed rate coefficients is not expected. The goal of these calculations is therefore to determine whether or not the experimentally observed product yields can be reproduced using this mechanism within the uncertainties of the calculations.

3.2.1. $C_2H_5O_2^\bullet + HO_2^\bullet$

Fig. 1 shows that Path I and Path II are both exothermic, and may be competitive with each other. However, once **5** is formed, decomposition back to **1** + **2** is lower in energy than reaction Paths III and III′. Intuitively, therefore, it is expected that only Path I will be important, and that ethyl hydroperoxide will be the major reaction product. To confirm this, Master equation calculations were carried out on Paths II, III, and III′. Chemically activated **3** (formed from the reaction **1** + **2**) is found to either decompose promptly back to **1** + **2**, or become thermally stabilized. To determine the fate of the collisionally deactivated **3**, kinetic simulations were carried out using FACSIMILE. **3** is found to equilibrate rapidly with the hydrotetroxide (**5**), but the forward reaction of **5** via **TS11** and **TS17** is found to be much slower than the reverse reaction of **3** to regenerate **1** + **2**. This reverse reaction occurs on a timescale of milliseconds, hence **3** and **5** likely do not survive long enough to undergo secondary bimolecular reactions. These calculations therefore support the experimental observation of ethyl hydroperoxide as the major product from the $C_2H_5O_2^\bullet + HO_2^\bullet$ reaction (Table 1).

3.2.2. $CH_3C(O)O_2^\bullet + HO_2^\bullet$

The product distribution from the reaction of acetyl peroxy radicals with $HO_2^\bullet$ is likely to be more complex than for the corresponding reaction of ethyl peroxy radicals because Paths I-A–IV-A are all exothermic (Fig. 3). Table 2 summarizes the branching ratios calculated in these simulations. Initially, the relative rates of Paths I-A and II-A were determined. Relative rate constants were calculated as described above, and were corrected for the fraction of **3-A** and **6-A** that decomposes back to **1** + **2**. Using the barrier heights given in Fig. 3 (Simulation 1-A), the relative yields of products from Paths I-A and II-A are found to be 0.7:0.3. Further, these yields are found to be extremely sensitive to the relative energies of **3-A** and **6-A**.

Table 2
Summary of calculated branching ratios for the acetyl peroxy + $HO_2^\bullet$ (A Simulations) and acetonyl peroxy + $HO_2^\bullet$ (B Simulations) reactions

Simulation	Comments	Y_{R1a}	Y_{R1b}	Y_{R1c}
1-A	Energies as in Fig. 3 ($E_{3\text{-A}} = -11.4$ kcal/mol; $E_{TS17\text{-A}} = -10.3$ kcal/mol)	0.72	0	0.28
2-A	$E_{3\text{-A}}$ lowered from −11.4 kcal/mol to −12.4 kcal/mol; $E_{TS17\text{-A}} = -10.3$ kcal/mol	0.35	0	0.65
3-A	$E_{3\text{-A}}$ lowered from −11.4 kcal/mol to −12.4 kcal/mol and $E_{TS17\text{-A}}$ lowered from −10.3 kcal/mol to −11.3 kcal/mol	0.35	0.05	0.60
4-A	$E_{3\text{-A}}$ lowered from −11.4 kcal/mol to −12.4 kcal/mol and $E_{TS17\text{-A}}$ lowered from −10.3 kcal/mol to −12.3 kcal/mol	0.35	0.19	0.46
1-B	Energies as in Fig. 5 ($E_{3\text{-B}} = -13.15$ kcal/mol)	0.79	0	0.21
2-B	$E_{3\text{-B}}$ lowered from −13.15 kcal/mol to −15.15 kcal/mol	0.34	0	0.66

Thus, lowering the energy of **3-A** by 1 kcal/mol (Simulation 2-A) changes the branching ratio of I-A:II-A to 0.35:0.65. This demonstrates that the pathways are competitive, and that the mechanism is consistent with the experimental yield of peracetic acid from this reaction [10] (see Table 1). Since peracetic acid is only formed from Path I-A in the proposed mechanism, the experimental yield of **9-A** of 0.4 implies a branching ratio I-A:II-A of 0.4:0.6.

A combination of Master equation calculations and kinetic simulations were used to determine the yields of products reacting via Paths II-A, III-A, and IV-A. For Simulation 2-A, the majority of chemically activated **3-A** formed from **1-A** + **2** is found to decompose back to reactants. Of the remainder, 30% promptly forms $^\bullet$OH (**16**), O_2 (**10**) and acetoxy radicals (**13-A**) via Path III-A, and 70% is collisionally stabilized as **3-A**. Once thermalized, **3-A** forms the hydrotetroxide **5-A**, which decomposes exclusively via Path III-A to form **16**, **10**, and **13-A**. The predicted branching ratios for Y_{R1a}:Y_{R1b}:Y_{R1c} are therefore 0.35:0:0.65 for Simulation 2-A. Despite being higher in energy, Path III-A is faster than Path IV-A due to the higher entropy of the loose transition state leading to **13-A** + **14**. The proposed mechanism thus does not appear to be consistent with the 20% yield of acetic acid (**19-A**) observed experimentally [10] (see Table 1). Once again, however, the branching ratios are extremely sensitive to the barrier heights. When the energy of TS17-A is lowered by 1 kcal/mol (Simulation 3-A), Y_{R1a}:Y_{R1b}:Y_{R1c} changes to 0.35:0.05:0.60, and when lowered by an additional 1 kcal/mol (Simulation 4-A) Y_{R1a}:Y_{R1b}:Y_{R1c} becomes 0.35:0.19:0.46. Thus, within the uncertainties of the calculations, the mechanism is consistent with the observed product yields. Simulation 4-A predicts that about 70% of the radical products from Path III-A are formed from collisionally stabilized **3-A** rather than being formed promptly from chemically activated **3-A**. Further, the calculations predict that these thermal reactions occur on a timescale of hundreds of milliseconds. It therefore appears possible that two of the flash photolysis studies of this reaction, where the experimental timescales were tens of milliseconds [19,21], may not observe the effects of radical formation via Path III-A. It should be noted, however, that ozone formation is observed in all three previous flash photolysis studies [19,21,22]. These observations contradict the results of the calculations, which predict that ozone formation should only be observed in reference [22], where the experimental timescale of 400 ms is long enough to observe products formed more slowly from thermalized intermediates.

Since the high $^\bullet$OH radical yield from the $CH_3C(O)O_2^\bullet + HO_2^\bullet$ reaction reported in [10] has not yet been confirmed in other studies, calculations were performed to test the importance of this pathway. For $^\bullet$OH radical formation to be a minor pathway, Path IV-A must dominate over Path III-A. This is not the case even when the energy of **TS17-A** is lowered by 5 kcal mol^{-1}. Since this value is greater than the uncertainties associated with these calculations, the proposed mechanism is consistent with the $^\bullet$OH radical being a major product of the $CH_3C(O)O_2^\bullet + HO_2^\bullet$ reaction.

As an additional check of the validity of the proposed mechanism, the overall rate coefficient for the $CH_3C(O)O_2^\bullet + HO_2^\bullet$ reaction was determined. A value of 4×10^{-12} cm^3 molecule^{-1} s^{-1} was obtained for Simulation 4-A at 298 K, which is about a factor of three lower than the recommended literature value of 1.4×10^{-11} cm^3 molecule^{-1} s^{-1} [22]. Given that a barrier height reduction of 1 kcal/mol will increase the rate coefficient of an elementary reaction by about a factor of 10 at 298 K, the difference between the calculated and recommended rate coefficients is consistent with both the uncertainties in the calculations, and the magnitude of the energy adjustments in Simulations 2-A–4-A.

To further investigate the proposed mechanism, calculations were carried out to determine the pressure and temperature dependence of the product yields using the parameters in Simulation 4-A. Results from these calculations are shown in Fig. 7 and Table 3. As the pressure is reduced from 760 Torr

Table 3
Calculated temperature dependence of the branching ratios for the acetyl peroxy + $HO_2^\bullet$ and acetonyl peroxy + $HO_2^\bullet$ reactions using Simulation 4-A and Simulation 2-B, respectively

Reaction	Temperature (K)	Y_{R1a}	Y_{R1b}	Y_{R1c}
$CH_3C(O)O_2^\bullet + HO_2^\bullet$	250	0.20	0.55	0.25
	298	0.36	0.19	0.46
	350	0.83	0.004	0.16
$CH_3C(O)CH_2O_2^\bullet + HO_2^\bullet$	250	0.94	0	0.06
	298	0.34	0	0.66
	350	0.28	0	0.72

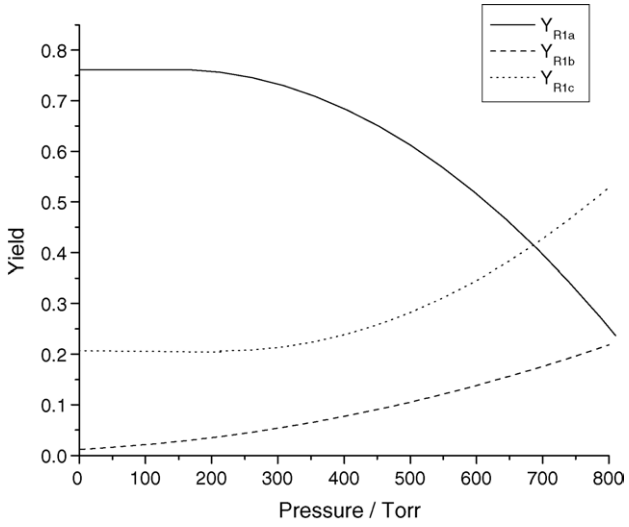

Fig. 7. Calculated pressure dependence of the branching ratios for the reaction of acetyl peroxy radicals with hydroperoxy radicals.

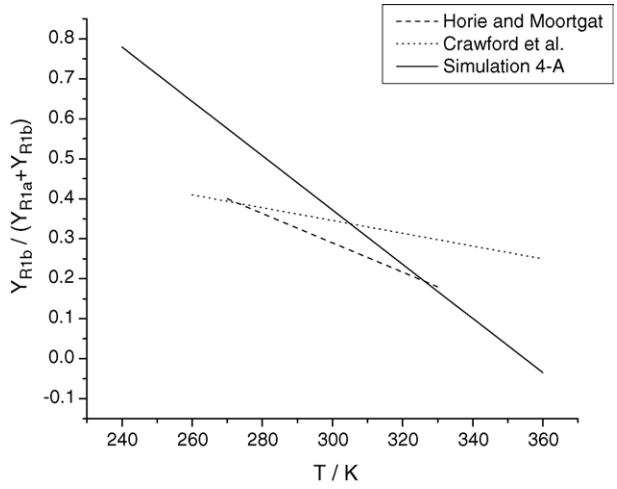

Fig. 8. Comparison of calculations with literature data for the temperature dependence of (R1a) and (R1b) in the reaction of acetyl peroxy radicals with hydroperoxy radicals. The data of Crawford et al. [21] have been corrected using the peracetic acid IR absorption cross-section of Orlando et al. [53] (see Section 3.2.2 for details).

to 1 Torr, the yield of peracetic acid increases from 0.35 to 0.78, while the yield of acetic acid decreases to less than 0.01, and the $^{\bullet}$OH yield decreases to 0.21 (Fig. 7). The reduction in pressure appears to have two effects. First, as the pressure is reduced, the fraction of 'hot' **3-A** decomposing back to **1-A** and **2** increases, leading to a decrease in the yield of products from Path II-A and a corresponding increase in the yield of peracetic acid. Second, as the pressure is decreased, the fraction of thermalized **3-A** also drops. Since acetic acid appears to be formed almost exclusively from collisionally stabilized **3-A**, the yield of this product decreases more quickly than that of the radical products from Path III-A, which can be generated from 'hot' **3-A**.

Table 3 shows the predicted variation in product yields with temperature. At 250 K, formation of thermalized 3-A via Path II-A is faster than formation of peracetic acid from Path I-A. At this temperature, thermal decomposition of **3-A** to form acetic acid is faster than radical formation via Path III-A, and so acetic acid is the major product. As the temperature increases, reactions via Paths I-A and II-A both become slower, but the rate coefficient of II-A decreases more rapidly with temperature. Thus, at 350 K, peracetic acid from Path I-A is the major product. Further, at higher temperatures, the yield of thermalized **3-A** decreases rapidly. As discussed above, collisionally stabilized **3-A** is the major source of acetic acid, and so as the temperature increases, the yield of this product rapidly decreases.

Four experimental studies have measured the relative branching ratios of Y_{R1a} and Y_{R1b} as a function of temperature. These studies are not in good agreement with each other. Tomas et al. [22] and Moortgat et al. [19] both report no temperature dependence for the branching ratios measured using the flash photolysis technique. On the other hand, Horie and Moortgat [20] report a strong negative temperature dependence for the quantity $Y_{R1b}/(Y_{R1a} + Y_{R1b})$ using matrix isolation FTIR spectroscopy. Crawford et al. [21] report a weak negative temperature dependence for this quantity using a combination of flash photolysis and FTIR measurements. However, the authors used a value for the IR absorption cross-section for peracetic acid that is three times smaller than the currently accepted value [53], leading to an underestimation of both Y_{R1b} and the temperature dependence of $Y_{R1b}/(Y_{R1a} + Y_{R1b})$. The calculations performed here indicate that the discrepancies between these studies may be a consequence of the different timescales involved in the flash photolysis and FTIR measurements. Decomposition of thermalized **3-A** via Paths III-A and IV-A may not be complete by the end of the flash photolysis runs, whereas the FTIR experiments occur on timescales that enable products from these reactions to be observed. Further experimental work is clearly needed to resolve the discrepancies. The temperature dependence of $Y_{R1b}/(Y_{R1a} + Y_{R1b})$ for the two FTIR studies have been plotted along with the predictions from calculations performed in this work in Fig. 8. In this plot, the branching ratios from Crawford et al. [21] have been corrected using Orlando et al.'s more recent IR absorption cross-section for peracetic acid [53]. As can be seen from these plots, the calculations predict the same negative temperature dependence for this quantity, although the calculated temperature dependence is much stronger than that observed in the experimental studies. Nonetheless, the qualitative agreement with experimental observations provides further evidence in support of the proposed mechanism.

3.2.3. $CH_3C(O)CH_2O_2^{\bullet} + HO_2^{\bullet}$

Based on the mechanism presented in Fig. 5, it appears that the acetonyl peroxy + $HO_2^{\bullet}$ reaction may follow the same pattern as the ethyl peroxy radical reaction, with acetonyl

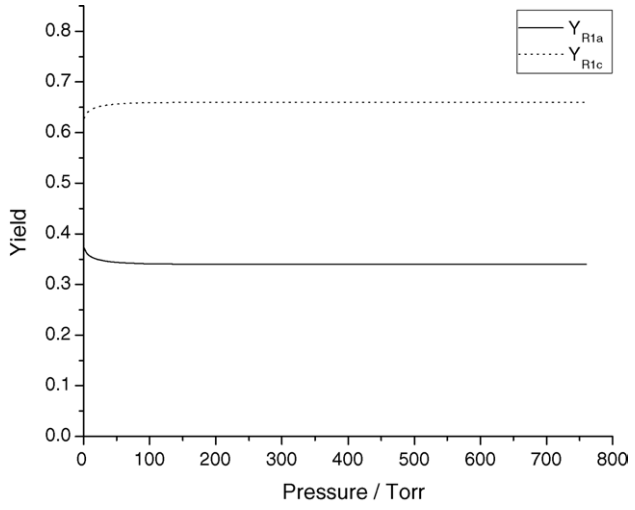

Fig. 9. Calculated pressure dependence of the branching ratios for the reaction of acetonyl peroxy radicals with hydroperoxy radicals.

hydroperoxide as the major product. Calculated product yields are summarized in Table 2. Using the barrier heights in Fig. 5 (Simulation 1-B), the calculations predict a branching ratio Y_{R1a}:Y_{R1c} of 0.79:0.21. Essentially all of the molecules reacting via Path II-B are collisionally deactivated to form thermalized **3-B**, which then rapidly equilibrates with the hydrotetroxide (**5-B**). Despite being slightly endothermic, decomposition via Path III-B′ to form 21-B and 10 is competitive with the reverse reaction, which regenerates 1-B and 2. As with the acetyl peroxy + $HO_2^\bullet$ reaction, the branching ratios for Paths I-B and II-B are sensitive to the energies of the hydrogen bonded intermediates **3-B** and **6-B**. Thus, lowering the energy of **3-B** by 2 kcal/mol (Simulation 2-B) gives a branching ratio Y_{R1a}:Y_{R1c} of 0.34:0.66, which is consistent with the experimentally measured product yields for this reaction [10] (see Table 1). The calculations indicate that the radical channel (R1c) proceeds through thermalized intermediates, and so the products are formed on a fairly slow timescale of 10^0 s or longer. This may explain the apparent discrepancy between the smog chamber measurements of Hasson et al. [10] which report (R1c) as the major product channel, and the flash photolysis study of Bridier et al. [54], which are consistent with (R1a) as the dominant reaction pathway.

Calculations were carried out to determine the temperature and pressure dependence of products formed via this mechanism. These data are shown in Table 3 and Fig. 9. The calculations predict that the product yields are essentially independent of pressure over the range 1–760 Torr (Fig. 9). At the lowest pressures investigated, the fraction of thermalized **3-B** begins to decrease, resulting in a slight decrease in the branching ratio for (R1c). In contrast, the temperature dependence is fairly pronounced, with an increase in the branching ratio for (R1c) as the temperature increases. As the temperature rises, Path III-B′ becomes increasingly labile, leading to an increase in the yield of radical products (Table 3). Thus, the increase in temperature is predicted to result in a decrease in the hydroperoxide yield, in contrast to the calculated prediction for acetyl peroxy radicals, where an increase in the hydroperoxide yield is expected. This apparent discrepancy is the consequence of the different mechanisms leading to the products of (R1c) for the acetyl peroxy and acetonyl peroxy reactions. To date, there are no experimental measurements of product yields as a function of temperature or pressure for comparison.

4. Conclusions

A mechanism has been proposed to explain the yields of products observed from the reaction of $HO_2^\bullet$ radicals with ethyl peroxy, acetyl peroxy, and acetonyl peroxy radicals. In this mechanism, the hydroperoxide (R1a) is formed via hydrogen atom transfer from $HO_2^\bullet$ to the $RO_2^\bullet$ radical. In contrast, both organic acids (R1b) and radicals (R1c) are generated via an organic hydrotetroxide. For the acetyl peroxy and acetonyl peroxy reactions, internal hydrogen bonding between the hydrotetroxide and the carbonyl group lowers the energy of intermediates and transition states to the extent that (R1c) becomes feasible. This reaction is also more thermodynamically favorable for the acetyl peroxy reaction due to stabilization of the resultant alkoxy radical by the adjacent carbonyl group. The hydrotetroxide formed in this reaction may also isomerize to form acetic acid and ozone (R1b). Significant fractions of the products formed via (R1b) and (R1c) are predicted to occur via thermal decomposition of stabilized intermediates rather than by prompt decomposition of chemically activated species. This suggests that product yield measurements from smog chamber studies and flash photolysis measurements, which typically are made on very different timescales, may not give the same results.

The mechanism proposed here for the acetyl peroxy + $HO_2^\bullet$ reaction is likely to be similar to that of larger acyl peroxy radical reactions. Reactions (R1b) and (R1c) therefore may occur for radicals of the general form $RC(O)O_2^\bullet$. Since larger species are collisionally deactivated more efficiently, these reactions are likely to occur thermally. The fact that the acetonyl peroxy radical + $HO_2^\bullet$ reaction can proceed via (R1c) due to internal hydrogen bonding raises the possibility that other organic peroxy radicals of the form $RCHXO_2^\bullet$ and $RCHXCH_2O_2^\bullet$ (where X is an electronegative atom) may also undergo this reaction. Future experimental work will test this hypothesis.

The calculations reported here have been used to predict the temperature and pressure dependence of the $RO_2^\bullet$ + $HO_2^\bullet$ product yields. Ultimately, the proposed mechanism can only be validated by experimental measurements. Therefore, additional smog chamber experiments will be carried out as a function of both temperature and pressure to provide a more rigorous test of the proposed reaction mechanisms.

Acknowledgments

A.S.H. and M.C.A. thank the College of Science and Mathematics, California State University Fresno for financial support of this work. K.T.K. and E. B. P. thank the donors of the American Chemical Society Petroleum Research Fund (#38037-GB6), the NSF Research Site for Educators in Chemistry at the University of Minnesota, the National Computational Science Alliance facility at the University of Kentucky (CHE040003), the University of Minnesota Supercomputing Institute, and the Violet Olson Beltmann Fund of Macalester College. K.T.K. also thanks Prof. Donald G. Truhlar (University of Minnesota) and his research group for their hospitality during a sabbatical visit during which much of this research was conducted.

References

[1] B.J. Finlayson-Pitts, J.N. Pitts, Chemistry of the Upper and Lower Atmosphere, Academic Press, San Diego, 2000.
[2] R. Atkinson, J. Phys. Chem. Ref. Data 26 (1997) 215–290.
[3] T.J. Wallington, S.M. Japar, Chem. Phys. Lett. 167 (1990) 513–518.
[4] T.J. Wallington, S.M. Japar, Chem. Phys. Lett. 166 (1990) 495–499.
[5] P.D. Lightfoot, P. Roussel, F. Caralp, R. Lesclaux, J. Chem. Soc., Faraday Trans. 87 (1991) 3213–3220.
[6] T.J. Wallington, J. Chem. Soc., Faraday Trans. 87 (1991) 2379–2382.
[7] T.J. Wallington, M.D. Hurley, Chem. Phys. Lett. 193 (1992) 84–88.
[8] M. Spittler, I. Barnes, K.H. Becker, T.J. Wallington, Chem. Phys. Lett. 321 (2000) 57–61.
[9] M.J. Elrod, D.L. Ranschaert, N.J. Schneider, Int. J. Chem. Kinet. 33 (2001) 363–376.
[10] A.S. Hasson, G.S. Tyndall, J.J. Orlando, J. Phys. Chem. A 108 (2004) 5979–6989.
[11] D.M. Rowley, R. Lesclaux, P.D. Lightfoot, B. Noziere, T.J. Wallington, M.D. Hurley, J. Phys. Chem. 96 (1992) 4889–4894.
[12] D.W. Gunz, M.R. Hoffmann, Atmos. Environ. 24A (1990) 1601–1633.
[13] A.V. Jackson, C.N. Hewitt, Crit. Rev. Environ. Sci. Tech. 29 (1999) 175–228.
[14] T.J. Wallington, M.D. Hurley, J.C. Ball, Chem. Phys. Lett. 211 (1993) 41–47.
[15] T.J. Wallington, M.D. Hurley, N.J. Schneider, J. Sehested, O.J. Nielson, Chem. Phys. Lett. 218 (1994) 34–42.
[16] V. Catoire, R. Lesclaux, N.J. Schneider, T.J. Wallington, J. Phys. Chem. 100 (1996) 14356–14371.
[17] T.J. Wallington, M.D. Hurley, N.J. Schneider, Chem. Phys. Lett. 251 (1996) 164–173.
[18] H. Niki, P.D. Maker, C.M. Savage, L.P. Breitenbach, J. Phys. Chem. 89 (1985) 588–591.
[19] G.K. Moortgat, B. Veyret, R. Lesclaux, Chem. Phys. Lett. 160 (1989) 443–447.
[20] O. Horie, G.K. Moortgat, J. Chem. Soc., Faraday Trans. 88 (1992) 3305–3312.
[21] M.A. Crawford, T.J. Wallington, J.J. Szente, M.M. Maricq, J.S. Francisco, J. Phys. Chem. A 103 (1999) 365–378.
[22] A. Tomas, E. Villenave, R. Lesclaux, J. Phys. Chem. A 105 (2001) 3505–3514.
[23] M.P. Sulbaek-Anderson, M.D. Hurley, T.J. Wallington, J.C. Ball, J.W. Martin, D.A. Ellis, S.A. Mabury, Chem. Phys. Lett. 381 (2003) 14–21.
[24] G.S. Tyndall, R.A. Cox, C. Granier, R. Lesclaux, G.K. Moortgat, M.J. Pilling, A.R. Ravishankara, T.J. Wallington, J. Geophys. Res. D 106 (2001) 12157–12182.
[25] H. Hou, B. Wang, J. Phys. Chem. A 109 (2005) 451–460.
[26] M.J. Frisch, G.W. Trucks, H.B. Schlegel, G.E. Scuseria, M.A. Robb, J.R. Cheeseman, J.A. Montgomery, J. Vreven, T. Kudin, K.N. Burant, J.C. Millam, J.M. Iyengar, S.S. Tomasi, J. Barone, V. Mennucci, B. Cossi, M. Scalmani, G. Rega, N. Petersson, G.A. Nakatsuji, H. Hada, M. Ehara, M. Toyota, K. Fukuda, R. Hasegawa, J. Ishida, M. Nakajima, T. Honda, Y. Kitao, O. Nakai, H. Klene, M. Li, X. Knox, J.E. Hratchian, H.P. Cross, J.B. Adamo, C. Jaramillo, J. Gomperts, R. Stratmann, R.E. Yazyev, O. Austin, A.J. Cammi, R. Pomelli, C. Ochterski, J.W. Ayala, P.Y. Morokuma, K. Voth, G.A. Salvador, P. Dannenberg, J.J. Zakrzewski, V.G. Dapprich, S. Daniels, A.D. Strain, M.C. Farkas, O. Malick, D.K. Rabuck, A.D. Raghavachari, K. Foresman, J.B. Ortiz, J.V. Cui, Q. Baboul, A.G. Clifford, S. Cioslowski, J. Stefanov, B.B. Liu, G. Liashenko, A. Piskorz, P. Komaromi, I. Martin, R.L. Fox, D.J. Keith, T. Al-Laham, M.A. Peng, C.Y. Nanayakkara, A. Challacombe, M. Gill, P.M.W. Johnson, B. Chen, W. Wong, M.W. Gonzalez, C. Pople, J.A., Gaussian 03, Gaussian Inc., Pittsburg, PA, 2003.
[27] C. Gonzalez, H.B. Schlegel, J. Chem. Phys. 90 (1989) 2154–2161.
[28] C. Gonzalez, H.B. Schlegel, J. Phys. Chem. 94 (1990) 5523–5527.
[29] J.A. Montgomery, M.J. Frisch, J.W. Ochteriski, G.A. Petersson, J. Chem. Phys. 110 (1999) 2822–2827.
[30] R. Gomez-Balderas, M.L. Coote, D.J. Henry, L. Radom, J. Phys. Chem. A 108 (2004) 2874–2883.
[31] D.J. Henry, C.J. Parkinson, L. Radom, J. Phys. Chem. A 106 (2002) 7927–7936.
[32] V. Guner, K.S. Khuong, A.G. Leach, P.S. Lee, M.D. Bartberger, K.N. Houk, J. Phys. Chem. A 107 (2003) 11445–11459.
[33] K.T. Kuwata, A.S. Hasson, R.V. Dickinson, E.B. Peterson, L.C. Valin, J. Phys. Chem. A 109 (2005) 2514–2524.
[34] A.S. Hasson, M.Y. Chung, K.T. Kuwata, A.D. Converse, D. Krohn, S.E. Paulson, J. Phys. Chem. A 107 (2003) 6176–6182.
[35] A. Dybala-Defratyka, P. Paneth, J. Pu, D.G. Truhlar, J. Phys. Chem. A 108 (2004) 2475–2486.
[36] M.L. Coote, G.P.F. Wood, L. Radom, J. Phys. Chem. A 106 (2002) 12124–12138.
[37] G.P.F. Wood, D.J. Henry, L. Radom, J. Phys. Chem. A 107 (2003) 7985–7990.
[38] T.I. Solling, D.M. Smith, L. Radom, M.A. Freitag, M.S. Gordon, J. Chem. Phys. 115 (2001) 8758–8772.
[39] A.E. Reed, R.B. Weinstock, F. Weinhold, J. Chem. Phys. 83 (1985) 735–746.
[40] J.R. Barker, Int. J. Chem. Kinet. 33 (2001) 232–245.
[41] J.R. Barker, MULTIWELL, 1.3.2, University of Michigan, Ann Arbor, 2003.
[42] K.T. Kuwata, K.L. Templeton, A.S. Hasson, J. Phys. Chem. A 107 (2003) 11525–111532.
[43] K.A. Holbrook, M.J. Pilling, S.H. Robertson, Unimolecular Reactions, Wiley, New York, 1996.
[44] J.R. Barker, N.F. Ortiz, Int. J. Chem. Kinet. 33 (2001) 246–261.
[45] FACSIMILE for Windows 3.0, UES Software.
[46] A. Padwa, J.M. Kassir, M.A. Semones, M.D. Weingarten, J. Org. Chem. 60 (1995) 53–62.
[47] I. Erden, F.-P. Xu, W.-G. Cao, Angew. Chem. Int. Ed. Engl. 36 (1997) 1516–1518.
[48] J. Barluenga, E. Rubio, A. Lopez-Pelegrin, M. Tomas, Angew. Chem. Int. Ed. Engl. 38 (1999) 1091–1093.
[49] J.J. Orlando, G.S. Tyndall, M. Bilde, C. Ferronato, T.J. Wallington, L. Vereecken, J. Peeters, J. Phys. Chem. A 102 (1998).
[50] L. Vereecken, J. Peeters, J.J. Orlando, G.S. Tyndall, C. Ferronato, J. Phys. Chem. A 103 (1999) 4693–4702.
[51] T.S. Dibble, J. Phys. Chem. A 108 (2004) 2199–2207.
[52] T.S. Dibble, J. Phys. Chem. A 108 (2004) 2208–2215.
[53] J.J. Orlando, G.S. Tyndall, L. Vereecken, J. Peeters, J. Phys. Chem. A 104 (2000) 11578–11588.
[54] I. Bridier, B. Veyret, R. Lesclaux, M.E. Jenkin, J. Chem. Soc., Faraday Trans. 89 (1993) 2993–2997.